CZECH TECHNICAL UNIVERSITY IN PRAGUE

FACULTY OF BIOMEDICAL ENGINEERING

Department of Natural Sciences

Biophysical characterization of non-motor contractility of actin cytoskeleton

Biofyzikální výzkum bezmotorové kontraktility aktinového cytoskeletu

Master thesis

Study program: Biomedical and Clinical Technology

Study branch: Instruments and Methods for Biomedicine

Thesis supervisor: Ing. Ondřej Kučera, Ph.D.

Consultant: Ing. Vladimíra Petráková, Ph.D.

Bc. Daniel Janda

Kladno, June 2019

ČVUT
ČESKÉ VYSOKÉ UČENÍ TECHNICKÉ V PRAZE

MASTER'S THESIS ASSIGNMENT

I. PERSONAL AND STUDY DETAILS

Student's name:	**Janda Daniel**	Personal ID number:	**474935**
Faculty:	**Faculty of Biomedical Engineering**		
Department:	**Katedra přírodovědných oborů**		
Study program:	**Biomedicínská a klinická technika**		
Branch of study:	**Instruments and Methods for Biomedicine**		

II. MASTER'S THESIS DETAILS

Master's thesis title in English:

Biophysical characterization of non-motor contractility of actin cytoskeleton

Master's thesis title in Czech:

Biofyzikální výzkum bezmotorové kontraktility aktinového cytoskeletu

Guidelines:

Actin cytoskeleton contractility plays an essential role in cell shape change and cellular motility. Although this contractility is usually contributed to the activity of myosin motors, recent observations revealed that there is another mechanism of actin contractility which serves either as a backup or a complement. The aim of this work is to characterise actin contractility propelled by diffusible crosslinkers. Specific instructions: 1. Design and perform experiments with a minimal model of actin contractility in the absence of molecular motors, using TIRF microscopy and reconstituted actin filaments. 2. Analyse temporal profiles of the contractions and design an analytical model of the phenomenon. 3. Reconstitute actin rings in the presence of diffusible crosslinkers and study their constrictions under varying properties of the buffers and stability of the filaments.

Bibliography / sources:

[1] M. Braun et al. , Changes in microtubule overlap length regulate kinesin-14-driven microtubule sliding, Nature Chemical Biology 13.12 , 2017, 1245 s.
[2] A. Lüdecke et al. , Diffusive tail anchorage determines velocity and force produced by kinesin-14 between crosslinked microtubules, Nature Communications 9.1 , 2018, 2214 s.
[3] M. Braun et al. , Entropic forces drive contraction of cytoskeletal networks, BioEssays 38.5 , 2016, 474-481 s.
[4] T. Cheffings et al. , Actomyosin ring formation and tension generation in eukaryotic cytokinesis, Current Biology 26.15 , 2016, R719-R737 s.
[5] A. Piekny and A.S. Maddox, The myriad roles of Anillin during cytokinesis, Seminars in Cell & Developmental Biology, ročník 21, číslo 9, 2010 s., Academic Press
[6] Z. Xue and A. M. Sokac, Back-to-back mechanisms drive actomyosin ring closure during Drosophila embryo cleavage, Journal of Cell Biology 215.3 , 2016, 335-344 s.

Name of master's thesis supervisor:

Ing. Ondřej Kučera, Ph.D.

Name of master's thesis consultant:

Ing. Vladimíra Petráková, Ph.D.

Date of master's thesis assignment: **03.05.2019**
Assignment valid until: **18.09.2020**

doc. Ing. Lenka Lhotská, CSc.
Head of department's signature

prof. MUDr. Ivan Dylevský, DrSc.
Dean's signature

ČVUT
ČESKÉ VYSOKÉ UČENÍ TECHNICKÉ V PRAZE

ZADÁNÍ DIPLOMOVÉ PRÁCE

I. OSOBNÍ A STUDIJNÍ ÚDAJE

Příjmení:	**Janda**	Jméno:	**Daniel**	Osobní číslo:	**474935**
Fakulta:	**Fakulta biomedicínského inženýrství**				
Garantující katedra:	**Katedra přírodovědných oborů**				
Studijní program:	**Biomedicínská a klinická technika**				
Studijní obor:	**Přístroje a metody pro biomedicínu**				

II. ÚDAJE K DIPLOMOVÉ PRÁCI

Název diplomové práce:

Biofyzikální výzkum bezmotorové kontraktility aktinového cytoskeletu

Název diplomové práce anglicky:

Biophysical characterization of non-motor contractility of actin cytoskeleton

Pokyny pro vypracování:

Kontraktilita aktinového cytoskeletu hraje zásadní roli ve změnách buněčného tvaru a v buněčné motilitě. Ačkoliv je typicky připisována aktivitě myozinových motorů, nová pozorování poukazují na přítomnost záložního mechanismu kontraktility, který nahrazuje či doplňuje příspěvek myozinů. Cílem práce je charakterizovat aktinovou kontraktilitu poháněnou difúzními spojníky. Pokyny pro vypracování: 1) Navrhněte a realizujte experimentální minimální model bezmotorové aktinové kontraktility s využitím TIRF mikroskopie a rekonstituovaných aktinových vláken. 2) Vyhodnoťte časové průběhy kontrakcí a vytvořte analytický model sledovaného fenoménu. 3) Rekonstituujte aktinové prstence za přítomnosti difúzních spojníků a studujte jejich konstrikce v závislosti na parametrech prostředí a stabilitě aktinových vláken.

Seznam doporučené literatury:

[1] Z. Xue and A. M. Sokac, Back-to-back mechanisms drive actomyosin ring closure during Drosophila embryo cleavage, Journal of Cell Biology, ročník 215, číslo 3, 2016, 335-344 s.
[2] T. Cheffings et al., Actomyosin ring formation and tension generation in eukaryotic cytokinesis, Current Biology, ročník 26, číslo 15, 2016, R719-R737 s.
[3] M. Braun et al., Entropic forces drive contraction of cytoskeletal networks, BioEssays, ročník 38, číslo 5, 2016, 474-481 s.
[4] A. Lüdecke et al., Diffusive tail anchorage determines velocity and force produced by kinesin-14 between crosslinked microtubules, Nature Communications, ročník 9, číslo 1, 2018, 2214 s.
[5] M. Braun et al., Changes in microtubule overlap length regulate kinesin-14-driven microtubule sliding, Nature Chemical Biology, ročník 13, číslo 12, 2017, 1245 s.
[6] A. Piekny and A.S. Maddox, The myriad roles of Anillin during cytokinesis, Seminars in Cell & Developmental Biology, ročník 21, číslo 10, 2010

Jméno a příjmení vedoucí(ho) diplomové práce:

Ing. Ondřej Kučera, Ph.D.

Jméno a příjmení konzultanta(ky) diplomové práce:

Ing. Vladimíra Petráková, Ph.D.

Datum zadání diplomové práce: **19.02.2019**
Platnost zadání diplomové práce: **18.09.2020**

doc. Ing. Lenka Lhotská, CSc.
podpis vedoucí(ho) katedry

prof. MUDr. Ivan Dylevský, DrSc.
podpis děkana(ky)

Declaration

I hereby declare that I have completed this thesis having the topic “Biophysical characterization of non-motor contractility of actin cytoskeleton” independently and I have included a full list of used references.

I do not have a compelling reason against the use of this thesis within the meaning of Section 60 of the Act No 121/2000 Sb., on copyright and rights related to copyright and on amendment to some other acts (The Copyright Act), as amended.

In Kladno date 16.05.2019 ……

Bc. Daniel Janda

Prohlášení

Prohlašuji, že jsem diplomovou práci s názvem „Biofyzikální výzkum bezmotorové kontraktility aktinového cytoskeletu" vypracoval samostatně a použil k tomu úplný výčet citací použitých pramenů, které uvádím v seznamu přiloženém k diplomové práci.

Nemám závažný důvod proti užití tohoto školního díla ve smyslu § 60 zákona č. 121/2000 Sb., o právu autorském, o právech souvisejících s právem autorským a o změně některých zákonů (autorský zákon).

V Kladně 16.5.2019 ……

Bc. Daniel Janda

Acknowledgement:

I would like to express my sincere gratitude to my supervisor Ondřej Kučera for the continual support of my master's thesis. I very much appreciate that I had an opportunity to work in an excellent science institute and had access to a cutting-edge technology.

Název diplomové práce:

Biofyzikální výzkum bezmotorové kontraktility aktinového cytoskeletu

Abstrakt:

Cytokineze je konečným krokem buněčného dělení, během kterého je mateřská buňka fyzicky rozdělena na dvě dceřiné buňky. Úspěch cytokineze závisí na utvoření kontraktilního prstence složeného z akto-myozinového cytoskeletu. Prstenec produkuje sílu potřebnou k rozdělení mateřské buňky. Navzdory obecně uznávaným předpokladům o kontraktilitě aktinu pomocí myozinových motorů dochází v některých buňkách ke kontrakci prstence, přestože je aktivita myozinu omezena. Cílem této práce bylo ověřit hypotézu, že kontraktilita aktinu může být poháněna bezmotorovým difuzním spojníkem anillinem. Použili jsme rekonstituovaná aktinová filamenta a anillin *in vitro* pro sudium minimálních modelů aktinové kontraktility bez přítomnosti myozinu. Pomocí TIRF mikroskopie jsme ukázali přímé nasouvání překrývajících se aktinových vláken a konstrikci aktinových prstenců. Naše výsledky ukazují, že anillin je difuzní spojník aktinových vláken a může přispívat k aktinové kontraktilitě.

Klíčová slova:

cytokineze, aktin, TIRF mikroskopie, anillin, molekulární spojníky

Title of the thesis:

Biophysical characterization of non-motor contractility of actin cytoskeleton

Abstract:

Cytokinesis is the final step of cell division during which the maternal cell is physically divided into two daughter cells. The success of the cytokinesis relies on the formation of the contractile ring composed of acto-myosin cytoskeleton. The ring produces the force required for the cleavage of the maternal cell. Despite the broadly accepted assumption that myosin motors are responsible for the actin contractility, in some cells, however, the ring contracts even when the activity of myosin is restricted. The aim of this thesis was to test the hypothesis that actin contractility can be propelled by diffusible nonmotor actin crosslinker anillin. We used reconstituted actin filaments and anillin *in vitro* to study minimal models of actin contractility in the absence of myosin. Using TIRF microscopy, we showed directional sliding of overlapping actin filaments and constriction of actin-anillin rings. Our results show that anillin is a diffusive crosslinker of actin filaments that may contribute to actin contractility.

Keywords:

cytokinesis, actin, total internal reflection fluorescence (TIRF) microscopy, anillin, molecular crosslinkers

Contents

Abbreviations

ABP: actin-binding proteins

ATP: adenosine triphosphate

CCD: charge coupled device

Da: Dalton (unit)

DDS: dichlordimethylsilane

F-actin: filamentous actin

GAB: general actin buffer

GFP: green fluorescence protein

IB: imaging buffer

NLS: nuclear localisation signal

OxSc: oxygen scavenger

PH: pleckstrin homology

Rho: Ras homolog gene family

ROK: Rho Kinase

TCE: trichloroethylene

TRITC: tetramethylrhodamine

List of figures

1 Introduction

The cytoskeleton consisting of protein-built filamentous structures has the responsibility for maintaining the cell shape, enabling cell migration and ensuring the cell division. A considerable part of the human cytoskeleton is made up of actin filaments with their associated proteins such as myosin. To understand cellular dynamics during, for instance, the cell division, the description of the mechanistic background of the cytoskeletal contractility is essential.

It is well known that myosin motors propel the actin contractility by translating one filament along another one. Despite this broadly accepted view, it remains unknown how the actin-myosin contractility mechanism ensures the proper functioning of certain physiological phenomena. The actin-myosin model alone fails, for instance, to explain constriction of the contractile ring, which consists of randomly oriented actin filaments. Suppose the myosin translates the filaments oriented in the opposite direction, this model will completely fail unless a symmetry breaking by another mechanism occurs. Furthermore, recent observations show that the presence of myosin motors is not necessarily required in some cells for the constriction of the ring and can be supported or fully replaced by another back-up mechanism.

In this thesis, I test the hypothesis that the actin contractility can be propelled by protein crosslinker anillin. Anillin is known to bundle actin filaments, and we assume that anillin acts as a diffusible crosslinker on these filaments and, therefore, generates compaction forces, which directionally slide partially overlapping filaments.

The aim of this thesis was to describe the contractile behaviour of reconstituted actin filaments crosslinked by anillin *in vitro* without the presence of molecular motors. To do so, I investigated the contractions of minimal anillin-actin systems and constrictions of reconstituted anillin-actin rings using TIRF microscopy.

Firstly, the behaviour of reconstituted rhodamine labelled actin filaments stabilised by phalloidin was observed as a control that the filaments do not interact with each other. Since anillin was added into the solution, we observed and assessed the directional sliding of the actin filaments along each other – the minimal model of non-motor actin contractility. Following experiments were aimed at the reconstitution of actin-anillin contractile rings under various conditions. Subsequent experiments tested similar situations but using non-stabilised actin filaments.

2 State of the Art

2.1 Biological background

2.1.1 Cytoskeleton

Cells adaptively interact with their surroundings. Cell shape change and development are ensured by the interplay of three types of filamentous protein structures called cytoskeleton [1]. This well-organised dynamic network is an essential component of eukaryotic cells and plays a major role not only in motility and morphogenesis, but also in intra-cellular transport, and cellular division [2].

The cytoskeleton is composed of intermediate filaments, microtubules, and actin filaments, also known as microfilaments [1]. The actin cytoskeleton is a dynamic network composed of actin filaments and a substantial number of other proteins having an ability to bind F-actin (filamentous actin). These proteins in many instances have several binding sites and are aimed at crosslinking the filaments, regulating their assembly and disassembly, and exerting force on the filaments [3].

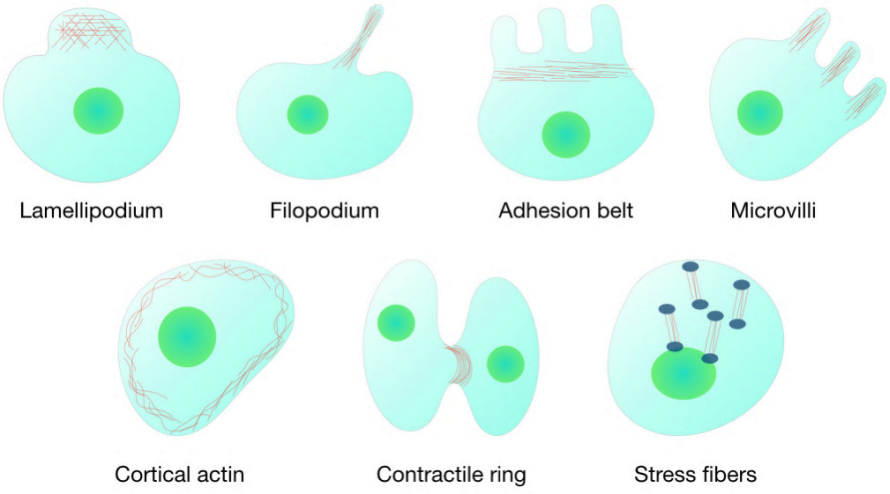

Figure 2.1 Actin filaments distribution in cells

Actin filaments have a considerable number of functions through cells. They can form many structures that play a broad range of roles such as enlargement of nutrient capacity (microvilli), the connection of cytoskeletal structures of adjacent cells (adhesion belt) and motility (lamellipodia, filopodia). Some of the actin-binding proteins exert forces on the actin stress fibres. Another function is ensured by the contractile ring, where the actin filaments contract and divide the cell into two daughter cells. Adopted from ref. [4].

2.1.2 F- actin structure and function

Actin is a highly conserved protein of 375 amino acids [5] with a mass of 42 kDa [6]. The globular actin has an ability to polymerise in a linear chain in the form of a single-stranded helix [7]. This filament has an approximate diameter of 8 nm and up to several microns in length. The fact, that the monomer position is always found to be in the same direction within the filament leads to the distinct structural polarity at both ends (so-called pointed end (–) and barbed end (+)) [8].

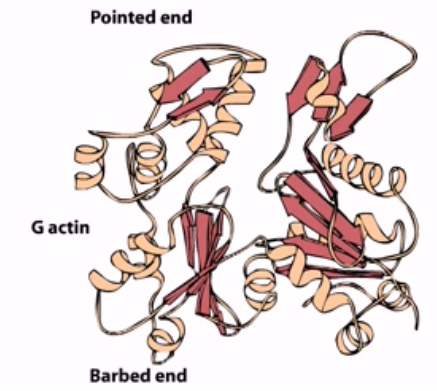

Figure 2.2 G-actin structure

A ribbon representation of a single G-actin monomer structure. A standard convention of the pointed end (upper part) and the barbed end (lower part) is used. Reprinted from ref. [1].

Actin polymerisation starts with the formation of the small trimer. Then actin filaments grow as other monomers are added to both ends, while the pointed end elongates slower than the barbed end. Actin binds ATP, which influences the rates of polymerisation. At the (+) end, there is usually a high concentration of the actin-bound ATP. Conversely, the (–) end has a high concentration of the actin-bound ADP. [8] Actin polymerisation and disassembly is regulated by a number of additional enzymes, such as profilin, cofilin and others [9].

Dynamic behaviour of the microfilaments and its interplay with associated proteins (also called actin-binding proteins, ABP) gives rise to the formation of higher-order structures such as bundles and networks [8].

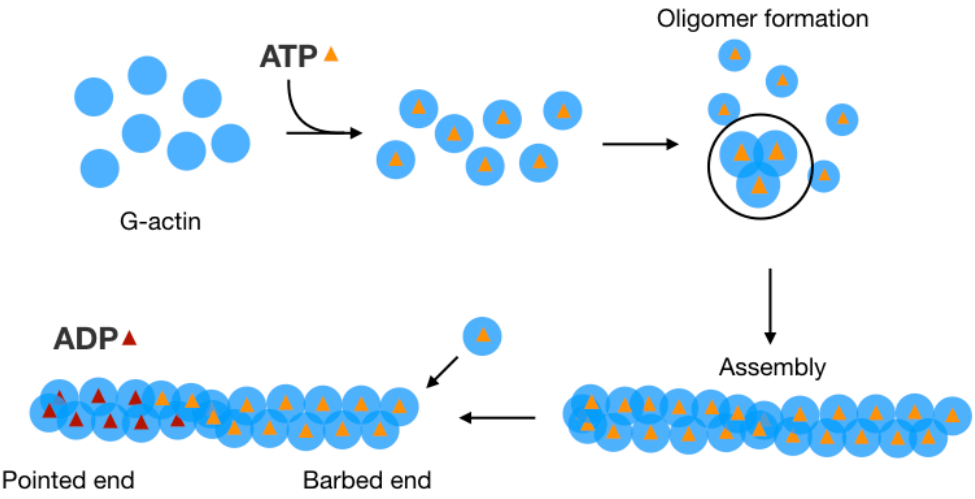

Figure 2.3 F-actin polymerisation

The polymerisation mechanism with the active participation of ATP leads to the formation of actin filaments by G-actin rearrangement. ATP is hydrolysed to ADP.

2.1.3 Actin contractility

Actin contractility plays a central role in cell motility and cell shape change. The myosin motors are mostly responsible for driving the actin contractility. Myosins act on the actin filaments by producing mechanical force by consuming chemical energy in the form of ATP. Hence a strain in the cytoskeletal network is produced because of the actin contraction. Apart from other structures, actin and myosin form a contractile ring closely anchored to the inner side of the cell membrane. In a generally accepted view, the myosin motor proteins within the contractile ring generate a constriction force for the physical cell division [2].

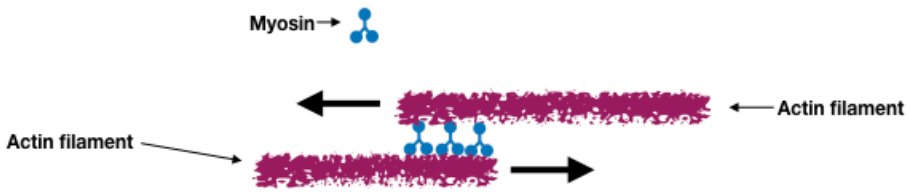

Figure 2.4 Actin-myosin contractility

The simplest actin-myosin contractile organisation consisting of two actin filaments forced to move by several motor protein units.

It is well known that myosin drives actin contractility. On the other hand, there are several problems with this model such as random orientation and arrangement of the actin filaments within the ring that can be shifted in opposite directions. When myosin acts on both parallel actin

filaments, no relative sliding occurs. Whilst antiparallel filaments can go from contraction to expansion depending on the initial geometry. This indicates that the model does not work with the exception of the presence of a backup or symmetry breaking mechanism [10].

Contractile ring is strictly regulated in terms of the precise timing of its localisation at the exact position to ensure equal distribution of the organelles and chromosomes. When a cell grows within the M phase and partitions the "mother" into two daughter cells, the cytokinetic failure is inadmissible. For this reason, when a cytokinetic failure occurs, it can lead to undesirable cellular malformations [11].

The assembly of the contractile ring is partly based on the Rho activation which then triggers actin polymerisation and myosin activation. On the other hand, Rho itself cannot change the actin protein conformation because Rho active GTP-bound state is required for the interaction. Rho-GTP promotes nucleation of actin filaments by activating mDia2 formins [11]. Its other function is to activate ROK and citron kinases to provide myosin assembly support [12].

Certain functions within the contractile ring are ensured by a number of other proteins, such as profilin, which accelerates actin filaments elongation and cofilin that plays a role in actin destabilisation. Both of these proteins are, therefore, the main participants in the assembly and disassembly dynamics of actin filaments. Another representative members of the group of additional proteins involved in the formation of the contractile ring are septins that are recruited by anillin, provide the anchorage of the ring to the membrane and, to some extent, control the stability of the contractile ring [11].

According to the classical model, once myosins utilise their motor activity, the actin filaments are forced to slide over each other, so the ring constricts. Interestingly, the cross-sectional area of the ring does not change with the constriction which leads to the assumption that the actin disassembly is synchronised with the constriction [11]. Furthermore, previous studies show that the rate of the constriction is proportional to the initial length of the boundary of the contractile ring [2, 11].

2.1.4 Anillin structure and function

Anillin is a protein with a molecular mass of 124 kDa, which binds actin, myosin and other key cytokinetic regulators. Anillin is also capable of interacting with a myriad of other proteins and is, therefore, regarded as a scaffolding protein. It can be usually found as a part of the contractile ring during cell division. This protein is able to bind actin and myosin through its conserved actin and myosin binding domain near its N-terminus. For this reason, anillin is sometimes referred to as the main cytoskeletal network coordinator. The actin-binding domain was found to have three individual actin binding sites (Figure 2.5) [13][14]. Conversely, near the C-terminus, the conserved PH domain resides. This domain plays a crucial role in anillin functionality by sharing homology with the Rhotekin, allowing to interact directly with RhoA [13][14]. Rho is another important small GTPase protein involved in the contractile ring formation and constriction which plays a fundamental role during the formation of the furrow where the anillin acts as significant co-operator and stabiliser [14].

In the absence of anillin in cells, the cytokinesis typically fails. Anillin knockout entails, for instance, the cleavage furrow failure, central spindle damage, contractile ring destabilisation, or oscillation of the contractile ring through a cell. This also suggests that anillin is responsible for furrow stability and is already present at the early stage of cytokinesis [14].

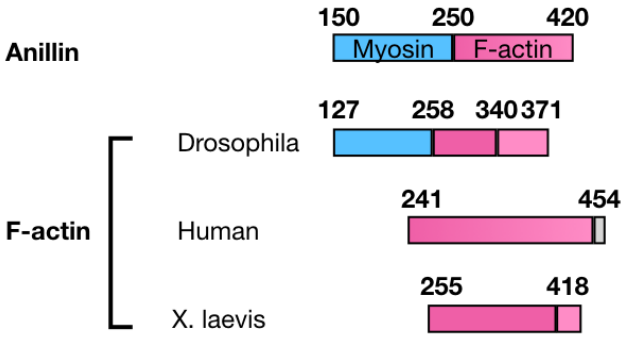

Figure 2.5 Anillin interaction domains

Anillin has several binding sites. Two of them are important in the context of this work - myosin and F-actin binding sites. Here a part of the human anillin structure and its interaction domains are shown. Black bars represent NLS sequences, and the numbering relate to the sequence of amino acids. Drosophila, Human and Xenopus represent the systems where the interacting protein was indicated [15].

2.1.5 Diffusible crosslinkers

While the generation of force by molecular motors (such as kinesin or myosin) is fuelled by the chemical energy released by the hydrolysis of nucleotides (such as ATP) [16], the cytoskeletal diffusible crosslinkers produce force by harnessing the thermal energy. The combination of the higher affinity of the crosslinker to the overlaps between cytoskeletal filaments and the one-dimensional diffusion along the filaments results in the confinement of crosslinkers in the overlaps. The thermodynamic tendency to maximise the entropy of the confined crosslinkers leads to the generation of forces that maximise the overlap length. This manifests by the directional sliding of the filaments. These forces can supplement the ATP-dependent forces and might be particular participants during the self-organisation of filamentous networks [17].

2.2 Technical background

2.2.1 Total Internal Reflection Fluorescence Microscopy

Total internal reflection fluorescence microscopy, TIRF, is a powerful imaging method bringing great contrast in the focal plane due to the suppression of excitation of fluorophores outside of this plane. This technique has a high signal-to-noise ratio compared to epifluorescence microscopic methods. As a secondary benefit, TIRF microscopy also reduces the extent of photodamage induced by the illumination laser. The source of illumination is a laser which comes in contact with a coverslip surface at a critical angle. Hence, the beam does not penetrate the

sample but only the evanescent wave propagates along the glass-sample interface. This wave excites fluorophores in the sample within a depth of approx. 100 nm from the coverslip surface. Thanks to the evanescent field, only the fluorophores that are close to the area of the surface are excited and observed, avoiding the background fluorescence from the volume [18].

The intensity of the evanescent field follows the expression

$$I(z) = I_0 e^{-(z/d_p)} \tag{1}$$

It decreases exponentially in a direction z with the characteristic depth of penetration (d_p). The penetration depth is described as

$$d_p = \frac{\lambda}{4\pi\sqrt{n_1^2 sin^2\varphi - n_2^2}} \tag{2}$$

It is a function of the wavelength (λ), of the indices of refraction of the glass and the solution and the angle of the incident light. See figure 2.6 for a graphic representation.

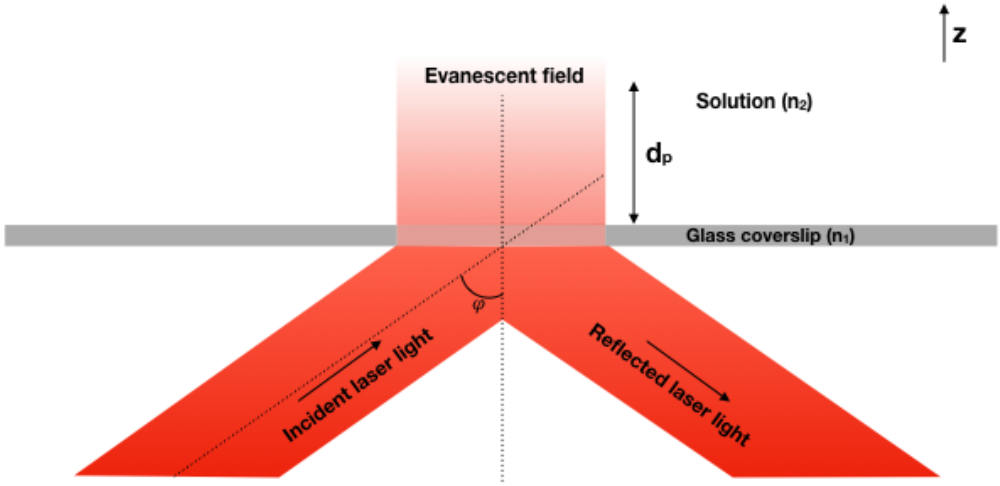

Figure 2.6 Optical geometry for total internal reflection fluorescence

The total internal reflection occurs when a critical angle φ is reached, thus the evanescent field is generated. Using equations 1 and 2, the light intensity and the penetration depth are described. Adopted from ref. [19].

Fluorescence microscopy allows us to see fluorophores below the resolution limit of light microscopy. And by substrate specific labelling it helps to resolve this substrate from other things in the image. Fluorochromes or fluorophores are the substances which are responsible for making objects of interest visible. The basic idea is that these substances are able to absorb light, and right

after the excitation, the electrons excited to the higher energy level return back to the lower energy level and emit the excess energy in the form of photons. These photons have lower energy than the excitation photons and thus longer wavelength compared to the excitation light beam. For the fluorescence excitation, specific light sources and detection devices are required [20].

The main difficulty of using fluorescence labelling is that fluorescence dyes have limited lifetime so they photobleach and, moreover, they may produce toxic substances [20]. By using specific reagents described at 4.1.2., the production of these substances can be restricted.

3 Materials and methods

3.1 Microscopy

In this chapter, techniques that were used for our experiments will be introduced.

3.1.1 Coverslips preparation

Following ref. [19], we prepared glass coverslips precisely cleaned to avoid undesirable fluorescence, and with the accurate reactivity for subsequent silanisation. The silanisation was completed with a 0.05% dimethyldichlorosilane (DDS) in the trichloroethylene (TCE) solution. This procedure was used to allow the glass surface functionalisation. It allows the surface passivation as well.

3.1.2 Fluorescent tag

For the "phalloidin-stabilised F-actin" experiments described in this work, we used rhodamine-phalloidin (tetramethylrhodamine) to make the actin filaments visible. While the phalloidin prevents F-actin from the depolymerisation (phalloidin), rhodamine is a fluorescent compound with the excitation/emission wavelength of about 540/565 nm. For the non-stabilised F-actin experiments we used rhodamine-actin without the use of phalloidin. We also used GFP-labelled anillin which can be excited by 488 nm laser light while the optimum of detection is at 510 nm (Figure 3.1).

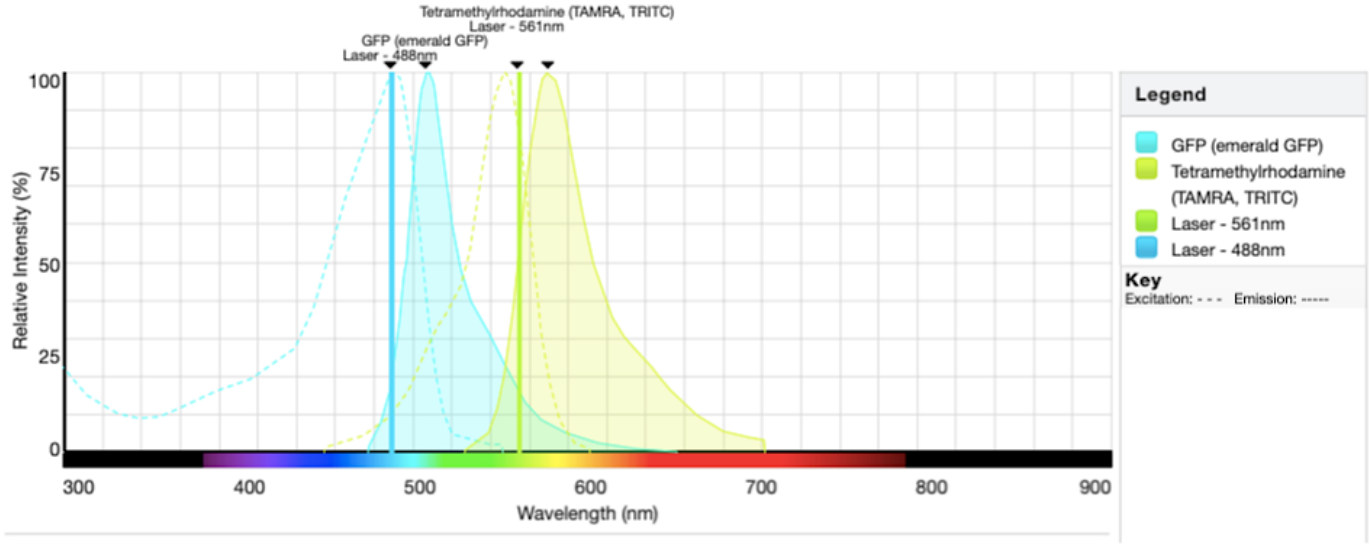

Figure 3.1 Fluorescent spectra

The fluorescent excitation and emission spectra of GFP and tetramethylrhodamine (TRITC) used in our experiments. The excitation lines indicate the wavelengths used to get the fluorophores to the excited state. By returning to the ground state, photons are emitted. The distance between the two maxima is known as the Stokes shift. Reprinted from ref. [21].

3.1.3 TIRF microscopy imaging setup

For the TIRF microscopy experiments, microfluidic chambers were prepared firstly. These chambers were formed from two 18x18 mm and 22x22 mm DDS coated glass coverslips while several approx. 1.5 mm wide parafilm strips were placed onto the bigger slide and the smaller slide was carefully pressed down onto the bigger one. This set was subsequently heated to approximately 65 ˚C to slightly melt the parafilm between the two slides to hold it together. The flow chamber was typically divided into four or five entry channels with a depth of approximately 100 μm. In Figure 3.2, I show the coverslip and its holder used for the experiments.

For studying actin-anillin behaviour during crosslinking, the coverslip surface was passivated by pluronic F-127 copolymer surfactant to avoid attaching actin filaments on.

For imaging, we prepared HEPES (20 mM HEPES, 2 mM MgCl2, 1 mM EGTA, pH 8.0 KOH) or GAB (5 mM Tris-HCl pH 8.0, 0.2 mM $CaCl_2$) buffer with the addition of Cleland's reagent (DTT), anti-photobleaching cocktail (glucose oxidase and catalase), and methylcellulose also called crowding agent.

This buffer contains HEPES or GAB, 10mM DTT, 20mM D-glucose, 0.1% Tween20, 0.5 mg/ml Casein, 1mM ATP. Then the solution was gently stirred, put on ice and placed in vacuum for degassing for at least 20 minutes.

Immediately before the start of filling the microfluidic chamber with the imaging buffer, glucose oxidase and catalase were added to the imaging mixture. It must be added just before use due to its extinction time of about 30 minutes. The importance of these two ingredients is based on the process of the oxidation of D-glucose to a gluconic acid that reduces the amount of reactive oxygen in the solution. A by-product of this reaction is hydrogen peroxide, which once again belongs to the undesirable reagents; therefore its amount is reduced by catalase [19].

Live imaging was performed using Nikon H-TIRF microscope with a CFI Apo TIRF 60x oil immersion objective, NA 1.49, working distance 0.12 mm (Nikon) while the sample holder was placed on the microscope stage and the glass coverslip was brought into contact with the objective by using immersion oil. Excitation wavelengths used for the experiments described below were 488 nm and 561 nm with laser beam power (LU - N4/N4S laser unit - Nikon) being set from 0,803 mW to 2,409 mW for 488 nm and from 0,856 mW to 2,568 mW for 561 nm which in both cases corresponds to the 10 - 30 % of the maximum laser power. The power was adjusted according to the intensity of the fluorescence signal. FITC and TRITC fluorescence filter cubes were used. The usage of separate filter cubes brings benefits for TIRF imaging, in terms of optimal filter selection, high experimental accuracy.

To record the fluorescence images the charge coupled device (CCD) camera (Andor Technology, iXon Ultra 888) and the NIS-elements acquisition software (Nikon) was used with a typical acquisition rate of approximately 1 frame per 200 milliseconds (actin sliding) and 1 frame per 10 seconds (actin rings). The actin-anillin sliding on experimental data was recorded by sequential switching between GFP and TRITC channels. The data was subsequently processed by the ImageJ software.

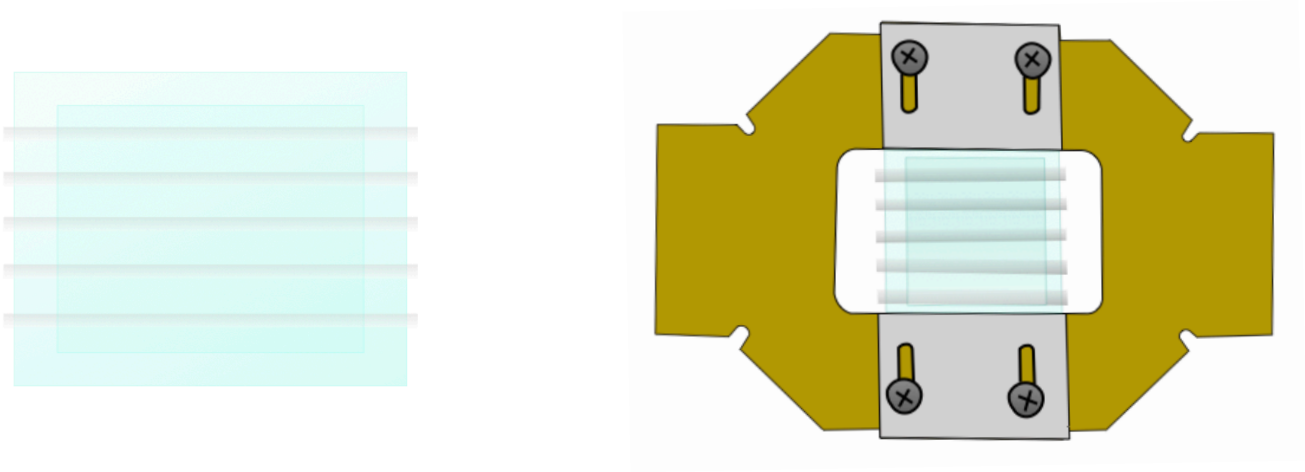

Figure 3.2 Microfluidic chamber and coverslip holder

a) Schematic representation of four microfluidic channels composed of 22 mm x 22 mm and 18 mm x 18 mm coverslips and five strips of parafilm. **b**) Custom-made copper coverslip holder with the central aperture used for placing the microfluidic chambers on the top of the microscope objective, which is able to approach the coverslip from underneath. The holders are precisely made to fit the microscope stage [19].

3.2 Acto-anillin interactions

We surveyed the interactions between the *in vitro* reconstituted F-actin and anillin. For the experimental investigations, we used actin filaments whose preparation is included in this chapter. We investigated how actin filaments were bundled in the presence of GFP-labelled anillin (Figure 3.3). We also investigated the directional sliding of individual actin filaments along each other. In subsequent experiments, we formed the acto-anillin rings and investigated their dynamics. The experiments were performed with phalloidin-stabilised and non-stabilised actin filaments.

The acetone powder protocols [22], [23] were used for the actin preparation. Then the protein was cryodesiccated and prepared to store at -80 °C for further use in our experiments. GFP-Anillin was prepared by recombinant protein production in HEK293 cells and stored at -80 °C.

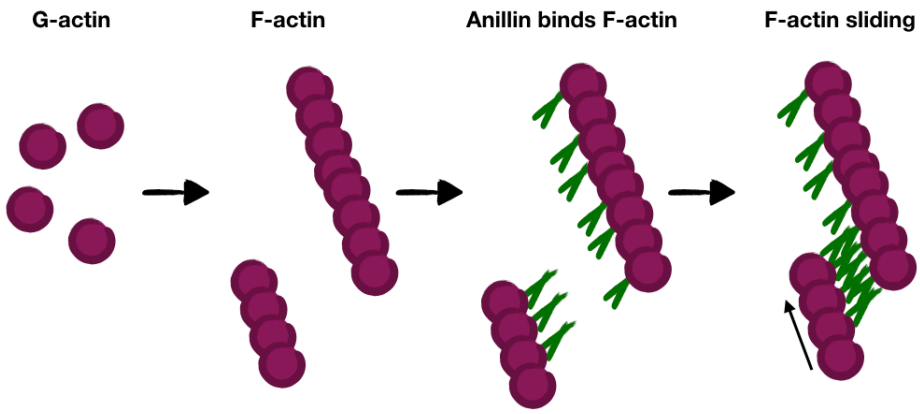

Figure 3.3 Phenomenological workflow of the experiments; from G-actin to F-actin sliding

From left; formation of F-actin from G-actin, anillin binding, and sliding of overlapping actin filaments.

3.2.1 Stabilised F - actin

Firstly, we polymerised actin filaments from globular actin. Once the actin filaments are formed, their depolymerisation may also occur. To prevent the depolymerisation, we used phalloidin, a chemical substance that binds and stabilises actin filaments.

Sliding of actin filaments

Filamentous actin was prepared from globular actin by spontaneous polymerisation in the polymerisation buffer (Attachment 1) in the presence of phalloidin. The actin filaments were left to polymerise at least until the next day prior to use. In the subsequent experiments, the flow sequence started with the coverslip surface passivation in each channel with pluronic F-127 for one hour. After this step, the channels were washed by the appropriate buffer in dependence on a buffer used afterwards. One of the channels selected for imaging was filled with actin filaments and the same channel was then flushed by the imaging buffer to which the oxygen scavengers and the last ingredient, the crowding agent, was added just before use.

The filaments were pressed down to the channel/glass interface by methylcellulose. Thanks to the passivation by F127, actin filaments were not adsorbed on the coverslip surface. In the result, the filaments were free to move in the lateral plane (see Figure 3.4).

Now, after putting the microscope into operation, we were able to observe actin filaments using the excitation wavelength of 561 nm.

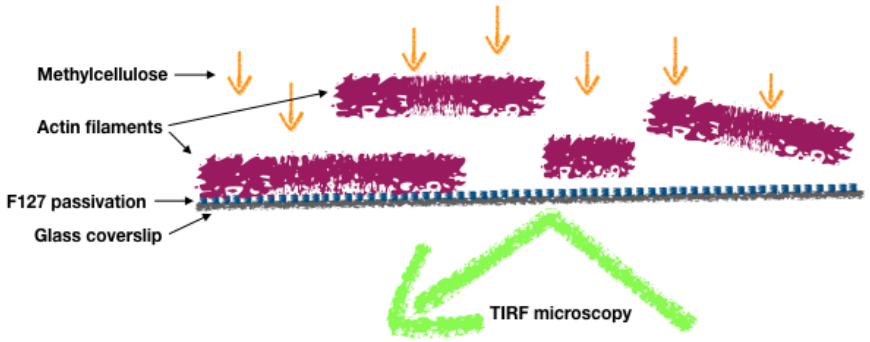

Figure 3.4 Actin filaments imaging setup

Schematic illustration of the setup for the TIRF microscopy imaging. Several actin filaments which are pressed down by methylcellulose onto the passivated coverslip surface and free to move along it are visible by fluorescence imaging, with an excitation wavelength of 561 nm. No interactions between these filaments were observed.

The actin filaments had a typical length of approximately 5-10 microns. For the following experiment, we added GFP-labelled anillin diluted (1:100) in the imaging buffer with methylcellulose and observed the interactions between anillin and F-actin. Observation of the anillin was possible with an excitation wavelength of 488 nm (Figure 3.5).

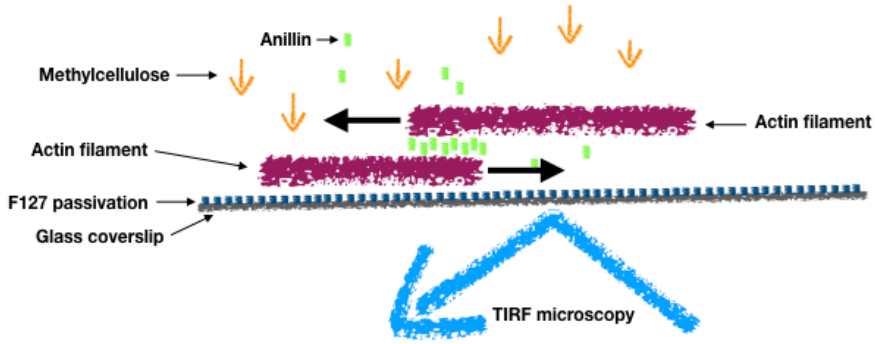

Figure 3.5 Minimal actin-anillin model imaging setup

Schematic illustration of the setup for the TIRF microscopy imaging. Two actin filaments, which are bound by GFP-tagged anillin and pressed down by methylcellulose onto the passivated coverslip surface, can be observed. Imaging is provided with an excitation wavelength of 488 nm.

Acto-anillin rings

The main difference between the previous procedure and this one is that the rings were prepared before they were injected into the channel. Firstly, actin filaments were prepared in the same way as described above, some of them were added into the micro-tube together with the imaging buffer containing anillin and oxygen scavengers. The crowding agent was added just before the channel filling. This procedure guaranteed the formation of acto-anillin rings (Figure 3.6) with which we were then able to fill the channel. After the channel was filled, we could observe those rings behaviour. With the exception of the acquisition rate, the microscope settings corresponded to the sliding-on experimental setting .

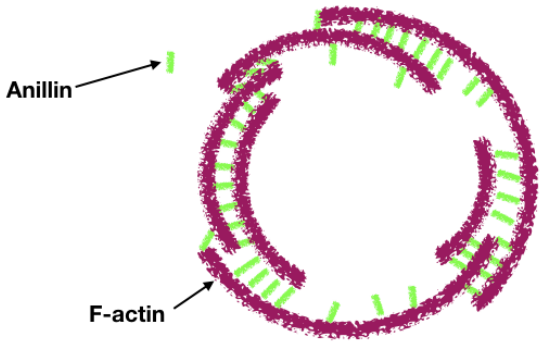

Figure 3.6 Actin-anillin ring

Illustration of an actin-anillin contractile ring composed of several actin filaments linked by anillin.

3.2.2 Non-stabilised F-actin

In the experiments with non-stabilised actin filaments, the addition of phalloidin was omitted. Under these conditions, slow actin depolymerisation occurs. It was observed how this phenomenon influences the interaction of actin filaments via anillin. For this type of experiment, a very important point is to use freshly prepared actin filaments to detect sliding of the filaments while the depolymerisation occurs.

Sliding of actin filaments

Actin filaments were prepared following the protocol in the Attachment 2. This actin was not prepared in our lab but prepared as a mixture of purchased rhodamine-labelled (AR05) and unlabelled (AKL99) actin at 1:10 ratio (Cytoskeleton, Inc., USA). The filaments were again placed into the microfluidic channel, were followed by imaging buffer containing oxygen scavengers and methylcellulose as described at the previous stabilised F-actin sliding-on

experiment. Right after the addition of the GFP-tagged anillin, image capturing was initiated. It was possible to see that the filaments slide along each other even during the process of depolymerisation.

Acto-anillin rings

We used the same preparation approach applied to the actin filaments as described in the previous section, to evaluate the differences between stabilised and non-stabilised contractile rings. Some of the filaments were added to the microtube and mixed with the solution of imaging buffer with OxSc and GFP-anillin (diluted 1:100). The rings were formed and after the addition of the methylcellulose, it could be transported to the microfluidic channel for observation. The procedure of monitoring differences in the ring dynamics is consistent with the procedure of the sliding-on experiment as mentioned above. According to our hypothesis, the size of the diameter of the non-stabilised rings should be highly affected by the gradual actin disassembly.

4 Results

This part is divided into three sections that deal with the contractions of minimal actin-anillin models, the density of anillin bound to the filaments, and the constrictions of reconstituted actin-anillin rings.

4.1 Actin-anillin contractions

We hypothesise that anillin can produce a force which can move actin filaments within a bundle. Therefore, we study the filaments in the presence of anillin to answer the question, whether or not do they slide along each other.

For the contraction experiments, phalloidin-stabilised actin filaments were used. In the presence of anillin, the situations of two actin filaments close to each other were recorded. It was noticed that anillin binds along these filaments uniformly. When coming into contact, a directional sliding was observed. Most of these observations were performed in HEPES buffer. I measured the length of the overlap of the two filaments as a function of the time, as the demonstrative curves show (Figure 4.3).

I also tested, whether the sliding on-phenomenon of non-stabilised actin filaments occurs under similar conditions as within the phalloidin-stabilised F-actin experiments.

4.1.1 Stabilised F-actin

Since phalloidin-stabilised actin filaments are spotted under the TIRF microscope, anillin is added into the solution in order to crosslink these filaments. Single filaments were visualised simultaneously with distinct 488 nm and 561 nm excitation wavelengths. The two filaments with a short distance between them were usually tracked. When touching, the sliding on each other could be observed. This was the typical behaviour through all of our experimental data. See Fig 4.1. and 4.2 for details.

Subsequent analysis revealed that the length of the overlap length increases rapidly at the beginning and asymptotically slows down as the time pass (Figure 4.3).

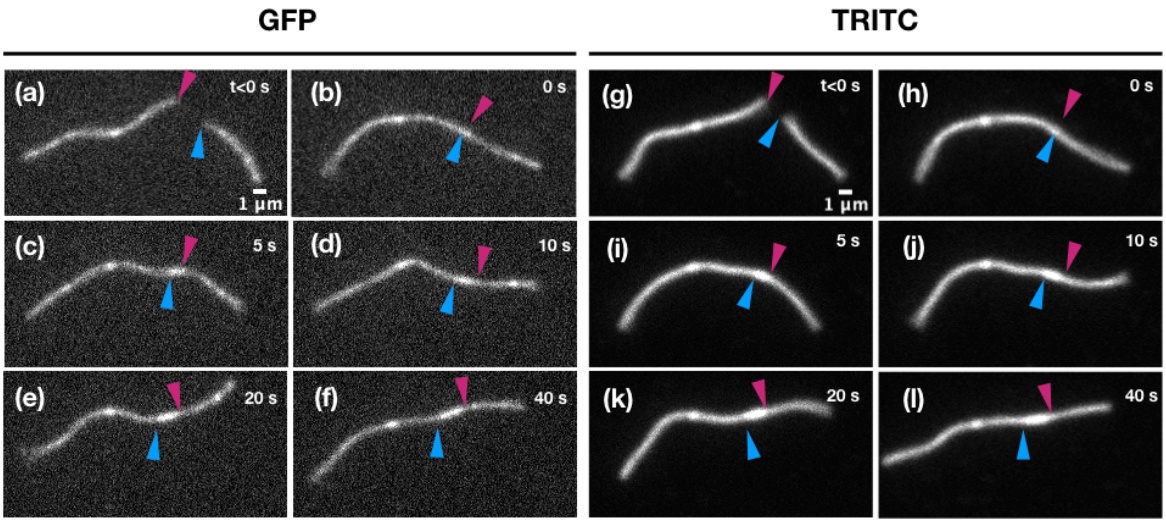

Figure 4.1 F-actin sliding in the presence of anillin

From (a) to (f): This figure shows the anillin-GFP channel with an excitation wavelength of 488 nm. Two phalloidin-stabilised actin filaments close to each other, when touching at t = 0 sec, are held together and able to move along each other over time. From (g) to (l): the same result in the TRITC channel, rhodamine-phalloidin, with an excitation wavelength of 561 nm is shown. The endpoints of the filaments that are in close proximity to each other are distinguished by coloured arrows. Each colour belongs to the individual filament. As the filaments move along each other in the opposite directions, the arrows follow the position of the endpoints. Thus, the length of the overlap can be directly measured afterwards. The spatial changes of the actin filaments between the GFP and the TRITC channels are given by the fact that actin filaments are free to move while the individual channels were recorded separately with a slight time delay.

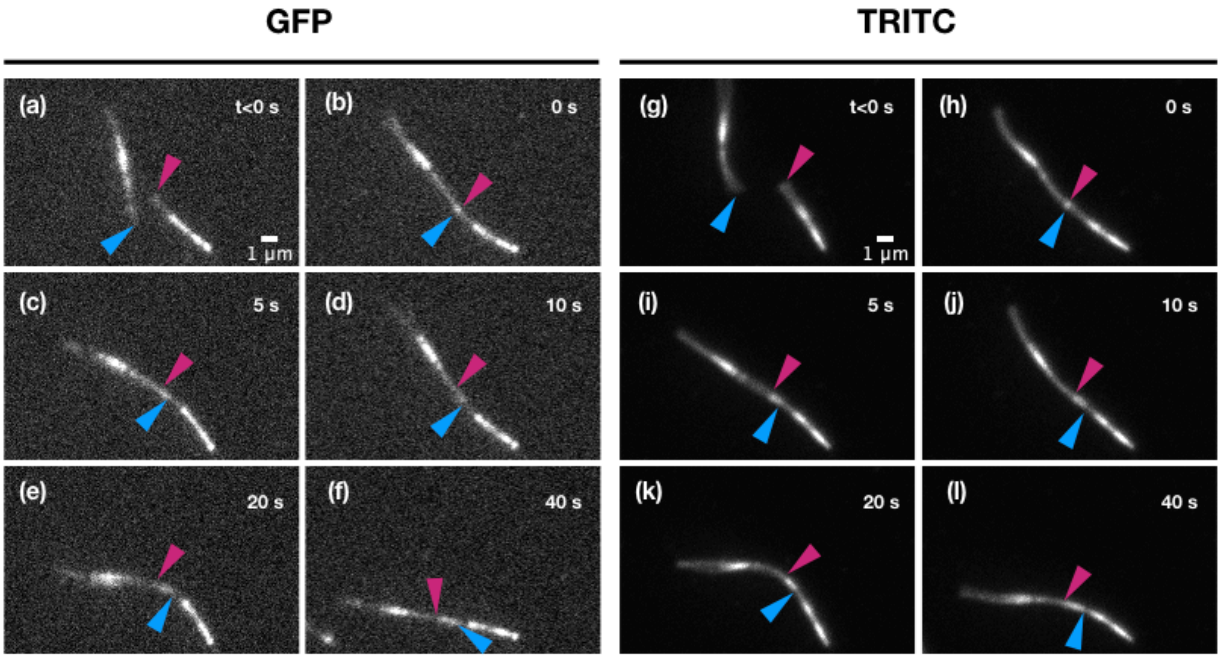

Figure 4.2 F-actin sliding in the presence of anillin

Another example of the actin filaments sliding on each other in the same setup as defined at the previous picture description.

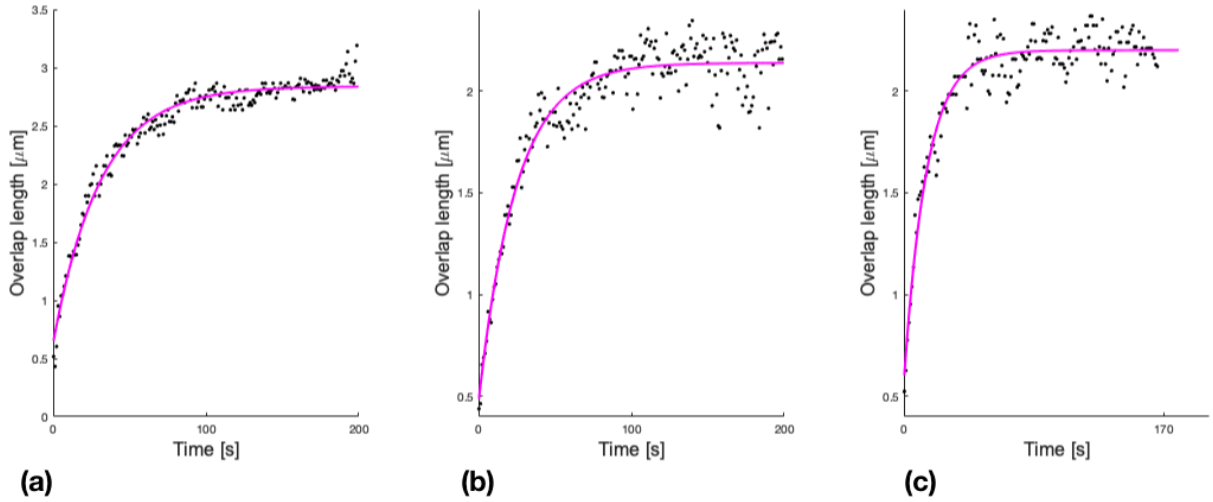

Figure 4.3 Actin-anillin sliding overlap length and time response

(a), (b) and (c) represent a typical behaviour of the directional sliding of actin filaments in the presence of anillin (Fig. 12. 13). In the majority of cases, the overlap length follows an exponential time response.

The control observations show that actin filaments are incapable of forming the bundles alone, without any additional protein in solution (Figure 4.4).

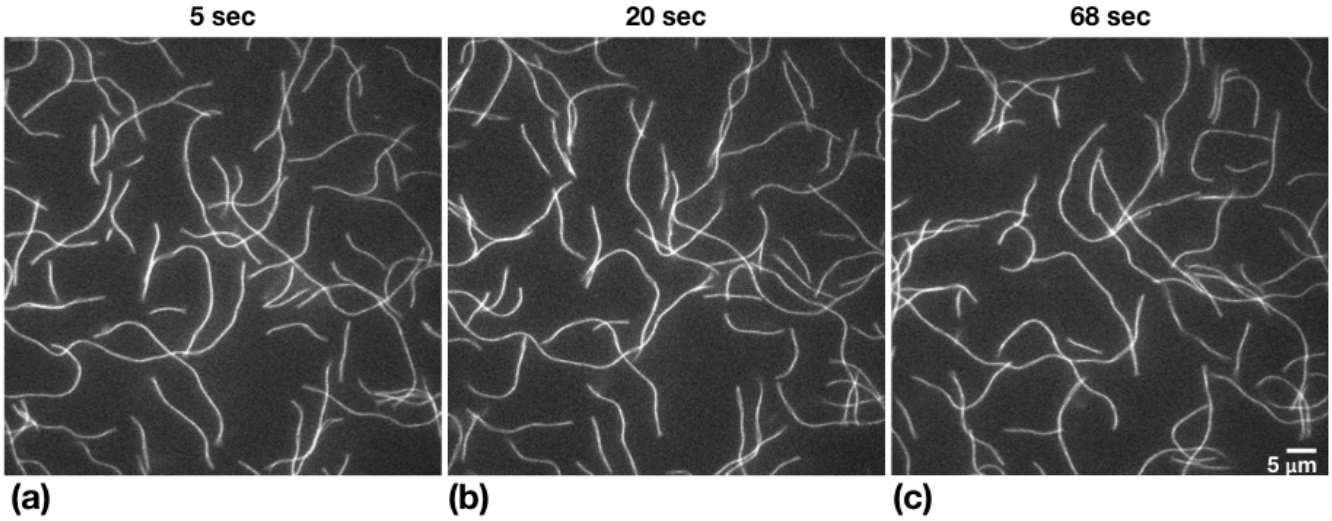

Figure 4.4 Actin filament cannot form bundles without anillin

Figures a, b, and c represent phalloidin-stabilised actin filaments at different times during one experiment. The filaments are free to move and occasionally touch each other. No long-term interactions such as sliding and alignment between those filaments can be observed.

4.1.2 Non-stabilised F-actin

Actin purchased from Cytoskeleton Inc. was used to answer the question of how the actin filaments move along each other while the depolymerisation occurs. I observed no difference in the behaviour; the filaments started to slide-on each other right after coming into contact. See Figure 4.5 for details.

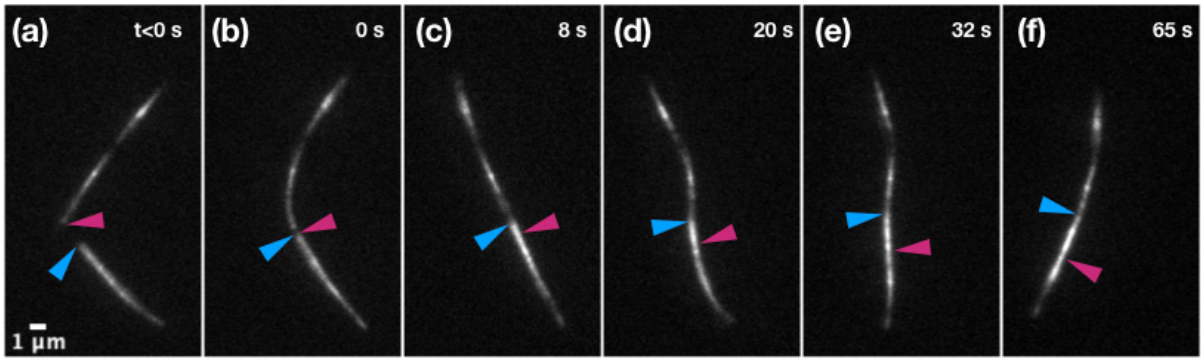

Figure 4.5 Sliding of non-stabilised actin filaments in the presence of anillin

Two actin filaments with the short distance between them are connected at the time of 0 secs (a, b). At the same time, they start sliding along each other as the blue and pink arrows show (c, d, e, f).

4.2 Anillin density

Next, we analysed the number of anillin molecules in the overlap. We suppose that the number of molecules of anillin grows together with the length of the overlap. Eleven measurements were tested in relation to this hypothesis. The analysis was done by quantification of the fluorescence intensity profile of GFP-anillin in the overlap. As Figure 4.6 shows, a pool of all the measurements can be fitted by a linear curve. By comparing the density of anillin in the overlap and on a single filament, we found that the density of anillin is approximately 1.6 times higher in the overlap.

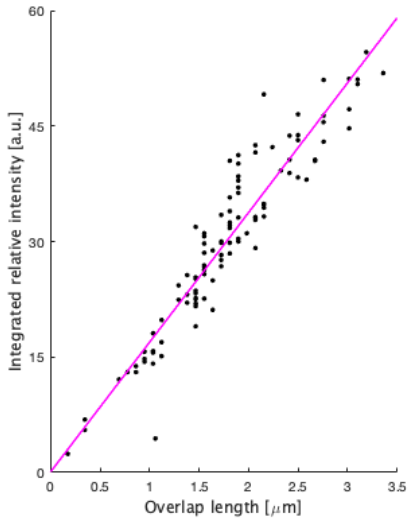

Figure 4.6 Anillin density as a function of the overlap length

The graph illustrates that the integrated relative intensity of the anillin follows the linear growth as the overlap length increases. There are 11 measurements included in the analysis.

For an example of the intensity profile used for the quantification of the anillin density in the overlap in the course of time, see Figure 4.7.

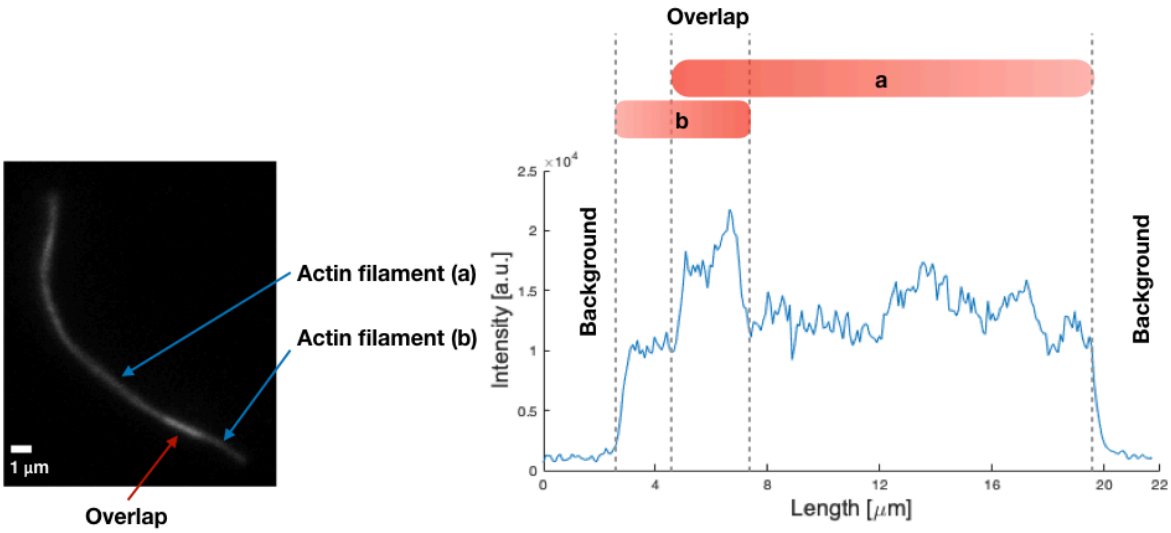

Figure 4.7 Intensity profile of two overlapping actin filaments

Two actin filaments (a) and (b) (on left) crosslinked by anillin in GFP channel. The graph on the right side of the figure shows the intensity profile along these filaments and also includes the background intensity. The grey bars stand for the individual segments of the profile.

4.3 Acto-anillin ring's constriction

In human cells, the formation of the contractile ring is ensured by remodelling of actin filaments. [24] Here we test the hypothesis that anillin contributes to the formation of contractile rings and produces constriction forces.

The rings composed of actin filaments crosslinked by anillin were prepared according to the description in the Materials and methods chapter. Similarly to the actin-anillin contractions experimental setup, I observed constrictions of the rings. Following figures 4.8, 4.10, 4.11 capture distinct rings in GFP and TRITC channels at different times.

The parameter that was found to be relevant for monitoring the contraction of the rings is the circumference, which was then plotted as the function of time. I also tested the rings under the different buffer conditions: the general actin buffer (GAB) and HEPES buffer.

Following sections 4.3.1, 4.3.2 contain the experimental situation or situations of individual actin rings. At the end of each section, there are the results of measured circumference in the course of time. On that basis, the constriction of the actin rings could be characterised. In many cases, the circumference decreases as the time pass, which means that the ring constricts. This is followed by a statistical analysis (4.3.3) which brings the information of how actin stability influences the constriction.

4.3.1 Stabilised F-actin

Once actin-anillin contractile rings were assembled from phalloidin-stabilised filaments, the individual rings could be tracked. See Fig 4.8 for the result of the single actin-anillin ring tracking. By measuring the circumference of the ring, it was evaluated whether the contraction occurs. Fig 4.9 shows that while some rings constrict, the constriction of other rings is less significant. Constriction of most of the rings was not able to exceed 5 %.

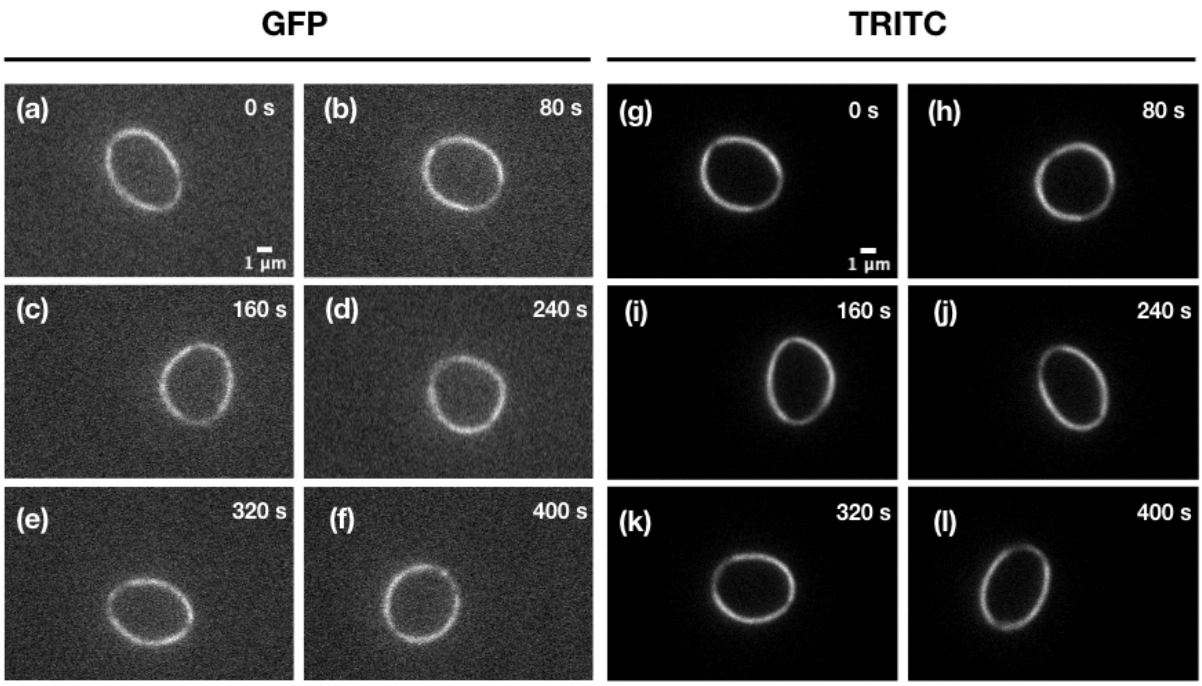

Figure 4.8 Phalloidin-stabilised actin-anillin contractile ring

Figures (a) to (f) show one contractile ring in the GFP channel at different times. Figures (g) to (l) show the identical contractile ring in the TRITC channel.

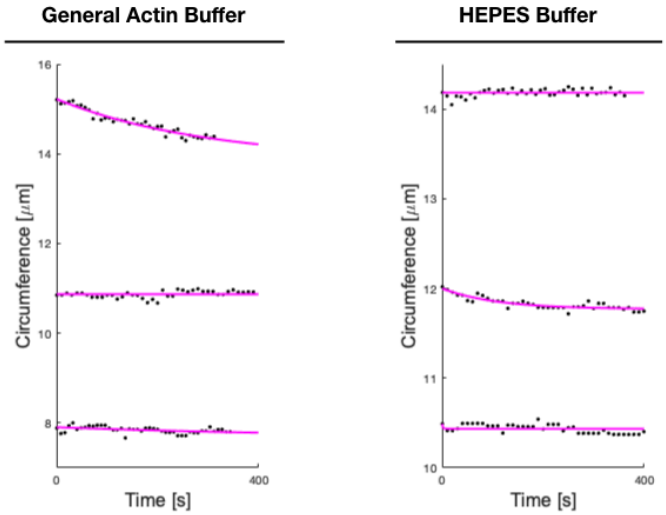

Figure 4.9 Constriction of actin-anillin rings in different buffers

The vertical axes show the circumference of the rings in the course of time. The buffers used are mentioned on the top of the images. Each curve represents an individual ring.

4.3.2 Non-stabilised F-actin

In this section, the non-stabilised actin rings are shown (Figure 4.10, 4.11). Once non-stabilised actin filaments were assembled, the actin-anillin rings could be formed in accordance with the experimental setup described in the chapter 3.2.2. Subsequent analysis revealed that the constriction of non-stabilised actin rings is approximately 52 % higher than phalloidin-stabilised actin rings.

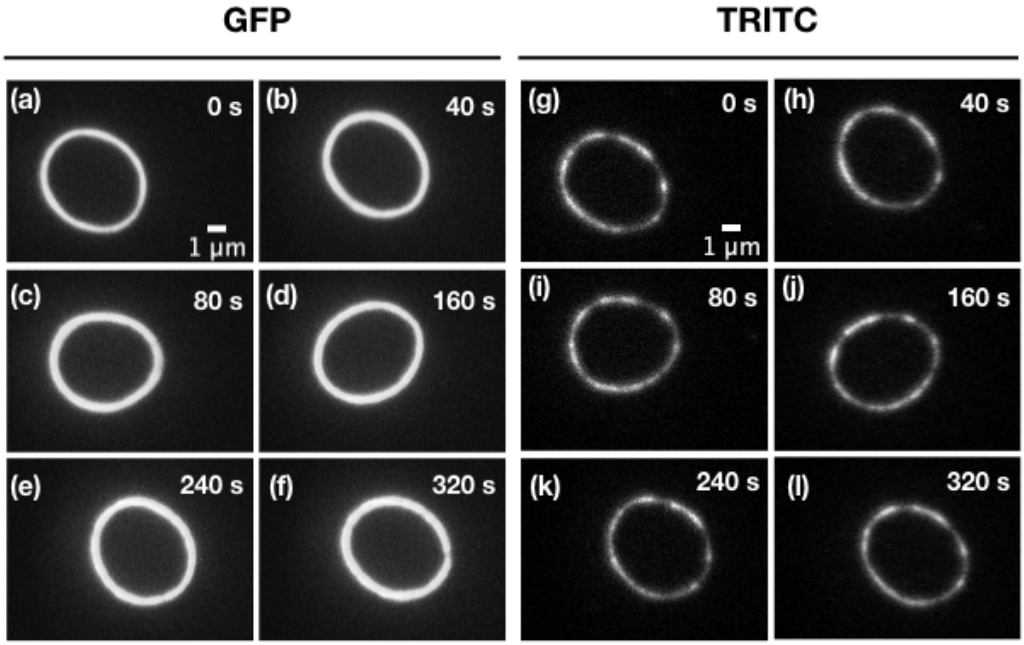

Figure 4.10 Non-stabilised actin-anillin contractile ring

A contractile ring in the GFP channel is shown in (a) - (f). Exactly the same contractile ring recorded in the TRITC channel (g) - (l).

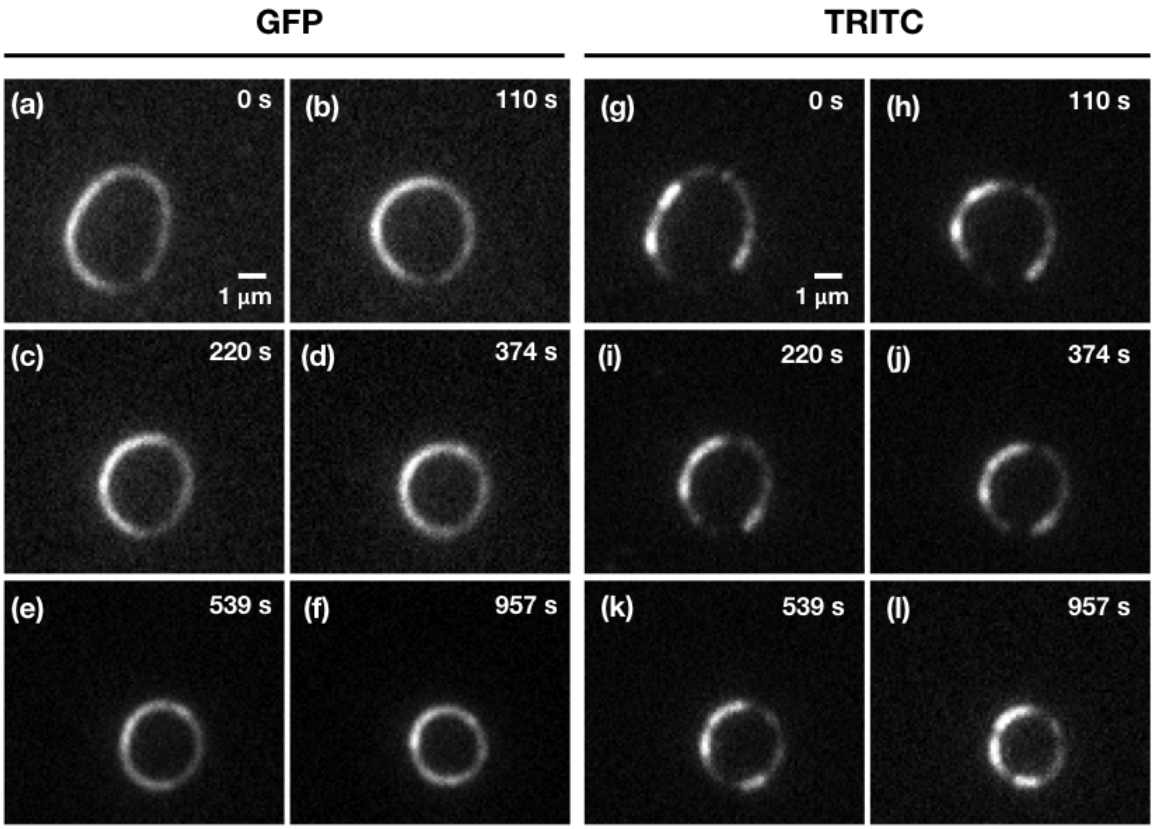

Figure 4.11 Non-stabilised actin-anillin contractile ring

A representative case of the non-stabilised actin-anillin contractile ring in both GFP (a-f) and TRITC (g-l) channels. Here the constriction phenomenon of the contractile ring can be observed just with a naked eye.

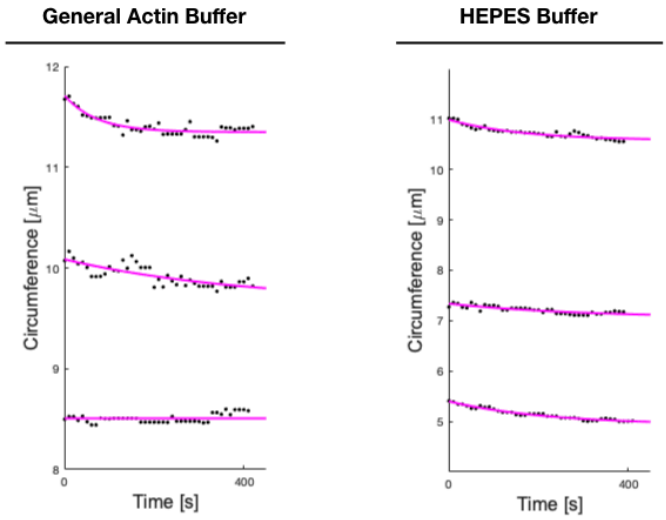

Figure 4.12 Constriction of actin-anillin rings in different buffers

An example of the time profiles of circumference of three representative events for each condition are shown. Each curve symbolises individual contractile ring within the single experiment.

4.3.3 Statistical analysis

Reconstituted actin-anillin rings constrict in the course of time. To assess this phenomenon, we analysed the rate of constriction under different experimental conditions. Firstly, we tested if there is a difference between data observed under different conditions. To do so, we tested whether our data come from the same distribution. The comparison was made with a two-tailed unpaired Student's t-test. The result is consistent with the hypothesis that there is no difference between the constriction rates of the rings in the two buffers, while the stability of the filaments has an influence on this rate. This allowed us to pool the results from different buffers and present the rates of constriction for stabilised and non-stabilised filaments (Figure 4.13). Contractile rings assembled of non-stabilised actin filaments have a higher contraction rate in relation to stabilised-actin rings.

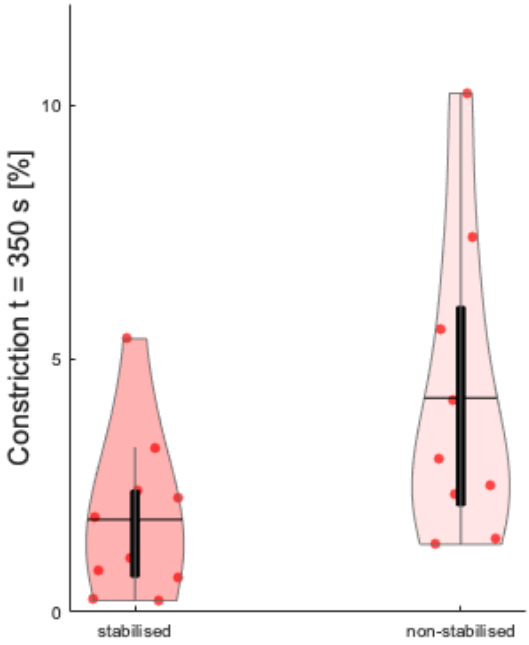

Figure 4.13 Constriction rate

Statistical comparation between stabilised (left) and non-stabilised (right) actin-anillin contractile rings. The vertical axis shows the percentage of constriction within the time of 350 s.

5 Discussion

The main goal of this work was to characterise actin contractility propelled by the diffusible crosslinker anillin. In this thesis, I showed that actin filaments are capable of moving along each other directionally in the absence of molecular motors, replaced with anillin.

The filaments were, in most cases, 5 to 25 μm in length, while the length depends on the actin polymerisation, in other words, on the concentration of free actin molecules in the solution. The visualisation of anillin-actin interactions was carried on simultaneously in channels with excitation wavelengths of 488 nm (GFP channel) and of 561 nm (TRITC channel). All the images were taken by continuous switching between the two lasers and by the periodical movement of the separation filter cubes which led to no crosstalk between those channels. The position of the identical actin filaments in both GFP and TRITC might be moderately, but not dramatically different due to the fact, that the filaments are free to move, and the filters cannot be switched instantly. Image acquisition could be carried out by simultaneous exciting of both GFP and TRITC fluorophores by both 488 nm and 561 nm lasers and using a beam splitter in the imaging line. Although such a design would prevent position changes between the channels, the beam splitter available in our lab does not have appropriated parameters. It would also reduce the image size by a factor of 2 and, therefore, reduce the yield of the experiments.

Rhodamine-tagged actin filaments were observed in 561 nm channel. Thanks to their low concentration, the individual filaments could be usually tracked. As the concentration of actin filaments increases, actin-anillin bundles can be formed. High concentrations of the filaments are thus inconvenient for single-filament tracking. Monitoring of actin filaments in the absence of anillin brings the results of no interaction between them (Figure 4.4). Since the addition of anillin, fluorescence signal became noticeable in the GFP channel. The 488 nm signal correlated with the 561 nm signal, proving that anillin binds the filament. Interestingly enough, in the GFP channel, the fluorescence signal was distributed equally from one end of the filament to the other. On this basis, we suggest that anillin binds F-actin uniformly.

Measuring the overlap length as a function of the time indicates that there is the exponential time response as show the curves in figure 4.3. In the beginning, the overlap length rapidly increases but the process slows down as the time pass. All of our experimental data follow a similar trend.

In cells, actin filaments dynamically polymerise as well as depolymerise. We assume that actin depolymerisation may positively affect the sliding of actin filaments in terms of creating additional space for further contraction as depicted in Figure 5.1 Our experimental data show that in the presence of anillin, the non-stabilised filaments slide along each other. We believe that further experiments based on this idea will reveal how actin disassembly influences the contraction rate and velocity.

It is well known that by consuming chemical energy in the form of ATP, molecular motors are able to promote the dynamic movement of cytoskeletal filaments. On the other hand, it was shown that cytoskeletal contractions can be driven by the entropic and enthalpic forces [17]. Since anillin is not a molecular motor and does not consume ATP, these forces could explain the contractions observed in our research.

Our *in* vitro experiments demonstrated that in the absence of molecular motors, actin filaments crosslinked by anillin slide over each other with an exponential time response. The overlap maximisation leads to the contraction of the bundle. Throughout the time of this process, the number of anillin molecules in the overlap increases linearly (Figure 4.11), suggesting that the contractions might be propelled by enthalpic forces produced upon binding of anillin to F-actin. Since the number of anillin molecules is higher in the overlap compared to a single filament, we can also speculate that the entropic forces may drive the contraction by rectifying the thermal energy [17]. Future research should resolve which of these mechanisms primarily drives the contraction.

We also observed *in vitro* formation of anillin-actin rings. By measuring the circumference of these rings, we analysed whether the contractions occur. Indeed, the majority of the rings in our experimental data constrict. The behaviour of the rings was investigated under different conditions. Two distinct buffers and two distinct types of actin filaments were used. Firstly, the rings consisting of phalloidin-stabilised filaments were experimentally studied in HEPES buffer, and then in general actin buffer. Secondly, the non-stabilised filaments were studied in identical buffers. By statistical analysis, it was proved that the behaviour of the individual contractile rings is consistent in both of these buffers for the same type of filaments. The rings formed by non-stabilised filaments proceeded further with the constriction.

It was explained above that the sliding of actin filaments driven by anillin lead to the overlap maximisation. We suppose that actin-anillin rings composed of several overlapping actin

filaments constrict in a similar fashion; the ring constricts as the bundle forming the ring contracts. Contractile rings formed of phalloidin-stabilised actin filaments have a lower contraction rate than rings assembled of non-stabilised filaments. This observation allows us to speculate that the constriction of the ring may depend on actin disassembly in terms of making the constriction easier by creating an extra space for further contraction (Figure 5.1).

It is well known that anillin colocalises with the contractile ring during cytokinesis. A number of examples was shown that cellular division can proceed in the absence of myosin or when the myosin motor activity is impaired [10]. We demonstrated that actin contractility can be propelled by a non-motor (thus ATP independent) actin crosslinker anillin. The contractile forces observed here are complemental to the activity of molecular motors.

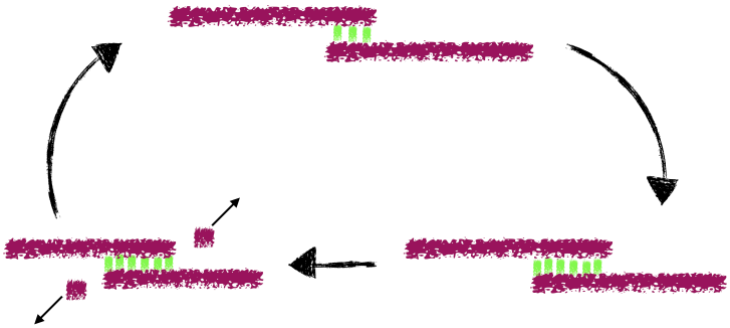

Figure 5.1 F-actin disassembly dynamics facilitates the sliding

The length of actin filaments decreases over time due to depolymerisation, which may create additional space for further contraction driven by anillin.

6 Conclusions

This work was aimed at *in vitro* study of interactions of actin filaments with actin cross-linker anillin to understand actin contractility without the participation of molecular motors.

Using TIRF microscopy, passivated microfluidic apparatus and reconstituted actin filaments we have shown that anillin uniformly binds these filaments. No changes in this binding were observed in the course of time. In the absence of anillin, no interactions between the filaments were observed. Upon addition of anillin, we observed formation actin bundles, confirming the crosslinking ability of anillin. We also observed that partially overlapping filaments were sliding-on and the overlap length between them was increasing.

To analyse the actin filaments sliding-on promoted by anillin, the overlap length between the filaments was directly measured. Through all of our data, the results show that the overlap length is an exponential function of the time, with rapid growth at the beginning and asymptotic slowing-down in the course of time. Subsequent quantitative analysis of the fluorescence intensity of GFP-anillin along the two overlapping filaments reveals that the density of anillin in the overlap is higher compared to the single filament by a factor of 1.6. Hence, we believe that GFP-anillin molecules may be confined in the overlap and can follow the characteristic behaviour of diffusible crosslinkers. The confinement may produce force in the direction of movement of actin filaments [25]. On that basis, we hypothesise that anillin is one of the actin-binding proteins which can harness thermal energy to generate force complementary to the myosin motors. On the other hand, the integrated relative intensity increases linearly as the two filaments slide along each other. Therefore, the number of anillin molecules scales linearly with the overlap length, suggesting that enthalpic forces can also contribute to the contractile behaviour. Further research should answer the contribution of entropic or enthalpic forces to this phenomenon.

We were able to observe the formation and contraction of actin-anillin rings *in vitro*. In the presence of anillin, a construct of two partially overlapping actin filaments usually contracts. In most cases, actin rings are formed of several overlapping actin filaments. Consequently, as the overlap length between the adjacent filaments increases, the ring contracts. It was shown that contractile ring assembled of phalloidin-stabilised actin filaments has a lower contraction rate in contrast to the one composed of non-stabilised filaments.

This is why we theorise that actin disassembly plays a role in the ring contraction. Our work provides an explanation, why the cytokinesis may proceed when the motor activity of myosin is impaired.

References

[1] ALBERTS, Bruce. *Molecular biology of the cell*. 5th ed. New York: Garland Science, 2008. ISBN 978-0-8153-4105-5.

[2] ZUMDIECK, Alexander, Marco Cosentino LAGOMARSINO, Catalin TANASE, Karsten KRUSE, Bela MULDER, Marileen DOGTEROM and Frank JULICHER. Continuum description of the cytoskeleton: Ring formation in the cell cortex. *Physical Review Letters*. 2005, **95**(25), 1–4. ISSN 00319007. doi:10.1103/PhysRevLett.95.258103

[3] FREEDMAN, Simon L., Shiladitya BANERJEE, Glen M. HOCKY and Aaron R. DINNER. A Versatile Framework for Simulating the Dynamic Mechanical Structure of Cytoskeletal Networks. *Biophysical Journal*. 2017, **113**(2), 448–460. ISSN 15420086. doi:10.1016/j.bpj.2017.06.003

[4] *How are actin filaments distributed in cells and tissues?* [online]. Available at: https://www.mechanobio.info/cytoskeleton-dynamics/what-is-the-cytoskeleton/what-are-actin-filaments/how-are-actin-filaments-distributed-in-cells-and-tissues/#how-are-actin-filaments-distributed-in-cells-and-tissues

[5] ELZINGA, M., J. H. COLLINS, W. M. KUEHL and R. S. ADELSTEIN. Complete Amino-Acid Sequence of Actin of Rabbit Skeletal Muscle. *Proceedings of the National Academy of Sciences*. 1973, **70**(9), 2687–2691. ISSN 0027-8424. doi:10.1073/pnas.70.9.2687

[6] ROBERTO DOMINGUEZ AND KENNETH C. HOLMES. Actin Structure and Function. *Annu Rev Biophys*. 2011, (3), 169–186. doi:doi:10.1146/annurev-biophys-042910-155359

[7] SANCHEZ, T., I. M. KULIC and Z. DOGIC. Circularization, photomechanical switching, and a supercoiling transition of actin filaments. *Physical Review Letters*. 2010, **104**(9), 65–68. ISSN 00319007. doi:10.1103/PhysRevLett.104.098103

[8] COOPER GM. *The Cell: A Molecular Approach* [online]. 2nd ed. Sunderland (MA): Sinauer Associates, 2000. Available at: https://www.ncbi.nlm.nih.gov/books/NBK9908/

[9] KUBOTA, Hiroaki, Makito MIYAZAKI, Taisaku OGAWA, Togo SHIMOZAWA, Kazuhiko KINOSITA and Shin'ichi ISHIWATA. Biphasic Effect of Profilin Impacts the Formin mDia1 Force-Sensing Mechanism in Actin Polymerization. *Biophysical Journal*. 2017, **113**(2), 461–471. ISSN 15420086.: doi:10.1016/j.bpj.2017.06.012

[10] CHEFFINGS, Thomas H., Nigel J. BURROUGHS and Mohan K. BALASUBRAMANIAN. Actomyosin Ring Formation and Tension Generation in Eukaryotic Cytokinesis. *Current Biology*. 2016, **26**(15), R719–R737. ISSN 09609822. doi:10.1016/j.cub.2016.06.071

[11] MILLER, Ann L. The contractile ring. *Current Biology*. 2011, **21**(24), R976–R978. ISSN 09609822. doi:10.1016/j.cub.2011.10.044

[12] PAOLO D'AVINO, P. How to scaffold the contractile ring for a safe cytokinesis - lessons from Anillin-related proteins. *Journal of Cell Science*. 2009, **122**(8), 1071–1079. ISSN 0021-9533. doi:10.1242/jcs.034785

[13] JANANJI, Silvana, Cristina RISI, Indeewari K.S. LINDAMULAGE, Louis Philippe PICARD, Robert VAN SCIVER, Guillaume LAFLAMME, Abe ALBAGHJATI, Gilles R.X. HICKSON, Benjamin H. KWOK and Vitold E. GALKIN. Multimodal and Polymorphic Interactions between Anillin and Actin: Their Implications for Cytokinesis. *Journal of Molecular Biology*. 2017, **429**(5), 715–731. ISSN 10898638. doi:10.1016/j.jmb.2017.01.020

[14] PIEKNY, Alisa J. and Michael GLOTZER. Anillin Is a Scaffold Protein That Links RhoA, Actin, and Myosin during Cytokinesis. *Current Biology*. 2008, **18**(1), 30–36. ISSN 09609822. doi:10.1016/j.cub.2007.11.068

[15] PIEKNY, Alisa J. and Amy Shaub MADDOX. The myriad roles of Anillin during cytokinesis. *Seminars in Cell and Developmental Biology*. 2010, **21**(9), 881–891. ISSN 10849521. doi:10.1016/j.semcdb.2010.08.002

[16] WOLLRAB, Viktoria, Raghavan THIAGARAJAN, Anne WALD, Karsten KRUSE and Daniel RIVELINE. Still and rotating myosin clusters determine cytokinetic ring constriction. *Nature Communications*. 2016, **7**(May), 1–9. ISSN 20411723. doi:10.1038/ncomms11860

[17] BRAUN, Marcus, Zdenek LANSKY, Feodor HILITSKI, Zvonimir DOGIC and Stefan DIEZ. Entropic forces drive contraction of cytoskeletal networks. *BioEssays*. 2016, **38**(5), 474–481. ISSN 15211878. doi:10.1002/bies.201500183

[18] WEBB, Rebecca L., Orr ROZOV, Simon C. WATKINS and Brooke M. MCCARTNEY. Using total internal reflection fluorescence (TIRF) microscopy to visualize cortical actin and microtubules in the Drosophila syncytial embryo. *Developmental Dynamics*. 2009, **238**(10), 2622–2632. ISSN 10588388. doi:10.1002/dvdy.22076

[19] CHRISTOPHER GELL, VOLKER BORMUTH, GARY J. BROUHARD, DANIEL N. COHEN, STEFAN DIEZ, CLAIRE T. FRIEL, JONNE HELENIUS, BERT NITZSCHE, HEIKE PETZOLD, JAN RIBBE, ERIK SCHÄFFER, JEFFREY H. STEAR, ANASTASIYA TRUSHKO, VLADIMIR VARGA, PER O. WIDLUND, MARIJA ZANIC, and Jonathon Howard. *Microtubule Dynamics Reconstituted In Vitro and Imaged by Single-Molecule Fluorescence Microscopy*. B.m.: Methods in Cell Biology. 2010. doi:10.1016/S0091-679X(10)95013-9

[20] DOBRUCKI, Jurek W. and Ulrich KUBITSCHECK. Fluorescence Microscopy. In: *Fluorescence Microscopy: From Principles to Biological Applications: Second Edition*. 2017. ISBN 9783527687732. doi:10.1002/9783527687732.ch3

[21] Fluorescence SpectraViewer. *Thermo Fisher Scientific* [online]. 2019. Available at: https://www.thermofisher.com/cz/en/home/life-science/cell-analysis/labeling-chemistry/fluorescence-spectraviewer.html

[22] EBASHI, Setsuro and Koscak MARUYAMA. Preparation and Some Properties of a-Actinin-free Actin. *The Journal of Biochemistry*. 1965, **58**(No. 1), 20–26.

[23] SPUDICH, James A and Susan WATT. The Regulation of Rabbit Skeletal. *the Journal of Biological Chemistry*. 1971, **246**(August 10), 4866–4871.

[24] SALBREUX, G., J. PROST and J. F. JOANNY. Hydrodynamics of cellular cortical flows and the formation of contractile rings. *Physical Review Letters*. 2009, **103**(5), 1–4. ISSN 00319007. doi:10.1103/PhysRevLett.103.058102

[25] LANSKY, Zdenek, Marcus BRAUN, Annemarie LÜDECKE, Michael SCHLIERF, Pieter Rein TEN WOLDE, Marcel E. JANSON and Stefan DIEZ. Diffusible crosslinkers generate directed forces in microtubule networks. *Cell*. 2015, **160**(6), 1159–1168. ISSN 10974172. doi:10.1016/j.cell.2015.01.051

List of attachments

Attachment A F-actin polymerisation

Table 1**:** Reagents and protocol

2x polymerisation buffer: 200mM KCl, 20 mM HEPES, pH 7.0
G-actin (4.5 mg/ml)
Rhodamin-phalloidin (125 µM in methanol) Sigma

1. Freshly resuspend dry rhodamin-phalloidin aliquot in 2 µl methanol.

2. 21.7 µl H_2O

   \+ 25 µl 2x polymerisation buffer

   \+ 1.3 µl G-actin (4.5 µg/ml)

   \+ 2 µl rhodamin-phalloidin in methanol (final 5 µM)

3. Incubate over night at 4°C

For an assay dilute approximately 1:10

Attachment B F-actin polymerisation (Cytoskeleton Inc.)

Table 2**: Reagents and protocol**

General Actin Buffer (5 mM Tris-HCl pH 8.0, 0.2 mM $CaCl_2$)
Muscle actin (10 mg/ml in General Actin Buffer and 0.2 mM ATP, 5% (w/v) sucrose and 1% (w/v) dextran)
10x polymerisation buffer (500 mM KCl, 20 mM $MgCl_2$, 10 mM ATP)
ATP 100 mM solution

Mix the reagents:

4 µl G-actin

96 µl GAB

0.5 µl ATP

10 µl 10x polymerisation buffer

For an assay dilute approximately 1:15

Attachment C Imaging buffer for F-actin

Table 3**: Reagents**

Volume	Reagent	Stock	Final
890 µl	HEPES	1x	
10 µl	DTT	1 M	10 mM
10 µl	D-glucose	2 M	20 mM
10 µl	Tween20	10% in BRB80	0.1%
50 µl	Casein	10 mg/ml	0.5 mg/ml
10 µl	ATP	100 mM	1 mM
20 µl	Glucose Oxidase and Catalase (10 µl of each, added later)		
1000 µl Final Volume			

Attachment D Imaging buffer with Oxygen Scavenger (always prepare fresh)

Table 4**: IB OxSc**

Volume	Reagent	Stock	Final
49 µl	IB	1x	
0.5 µl	Glucose oxidase	22.4 mg/ml	0.22 mg/ml
0.5 µl	Catalase	2 mg/ml	0.02 mg/ml
50 µl Final Volume			

Attachment E CD

Janda_abstrakt_cz.pdf

Janda_abstrakt_eng.pdf

Key_words.pdf

Assignment.png

Zadani.png

Janda_Master_thesis.pdf